Mesoscopic transport properties of 2D disordered metallic films: a proposal for the observation of Anderson localization

1991 J. Phys.: Condens. Matter 3 4257

(http://iopscience.iop.org/0953-8984/3/23/014)

J. Phys.: Condens. Matter 3 (1991) 4257–4267. Printed in the UK

Mesoscopic transport properties of 2D disordered metallic films: a proposal for the observation of Anderson localization

Ping Sheng and Zhao-Qing Zhang†
Exxon Research and Engineering Company, Route 22 East, Annandale, NJ 08801, USA

Received 8 February 1991

Abstract. We use the 2D quantum percolation model to simulate the mesoscopic transport properties of disordered metallic films. The conductance of a mesoscopic sample is calculated by the multichannel Landauer formula, with the transmission and reflection coefficients evaluated numerically with a recursive Green-function approach. The distribution of the conductance is found to exhibit three distinct types: normal, log–normal and between normal and log–normal, depending on the sample size L and metal fraction p. The variation of the mean with L yields the localization length and the root-mean-square conductance fluctuation Δg is shown to have different regimes, including the universal-conductance fluctuation regime where Δg is constant as a function of L and of the order of e^2/h. Based on these results, we propose the use of mesoscopic samples of disordered metallic films for the direct experimental observation of Anderson localization for electrons. Two possible sample systems are discussed.

1. Introduction

Mesoscopic is a term denoting the sample scale intermediate between the molecular scale and the bulk scale. For electronic transport, the importance of making this sample size regime distinct is that one can observe the effects due to phase interference of the electronic wavefunctions, and novel phenomena are expected. The recent discovery of universal conductance fluctuations [1] (UCF) is a good example. The primary motivation of this work is to examine the mesoscopic electronic transport properties of disordered 2D metallic films, and, based on the results obtained, to propose experiments for the direct observation of Anderson localization of electrons, conductance fluctuations, distribution of conductances and various regimes of metallic conduction. Two possible systems are envisaged: granular metal films and disordered 2D electron gases.

Granular metals are metal–insulator composites formed by co-sputtering or co-evaporation. They are mostly in the form of thin films less than 1 μm thick. Over the past two decades, the electrical tranport properties of granular metal films have been a topic of active experimental and theoretical study [2]. In the dielectric regime, where the metal grans are dispersed in an insulating matrix, electrical conduction is by the

† Also at Bartol Research Institute, University of Delaware, Newark, Delaware 19716 and Institute of Physics, Academia Sinica, Beijing, People's Republic of China.

0953-8984/91/234257 + 11 $03.50

hopping mechanism [3, 4] whereby the charge carriers are transported from grain to grain via thermally-activated tunnelling. In the metallic regime, on the other hand, electrons can percolate directly through connected metallic networks so that the conductivity is expected to exhibit normal metallic behaviour. However, due to the small size and random nature of the metallic channels, the electrons scatter strongly, which can lead to localization. Localization behaviour has indeed been observed indirectly in the metallic regime of granular metals. For example, at low temperatures the resistivity of granular metal samples increases logarithmically as the temperature decreases [5], indicating that as $T \rightarrow 0$ all electrons tend to be localized. Due to the indirect nature of such observations, however, a detailed picture of electron localization is impossible.

The advantages of using mesoscopic granular metal samples to observe Anderson localization are threefold. First, the electron density is high in the metal, which means that one can neglect electron–electron correlation effects and obtain a clean signature of the Anderson localization. Second, the volume fraction of the insulator is variable, which means that the material offers a handle on controlling the scattering strength; this makes it possible to encompass a broad range of localization characteristics, including the variation of localization length and the possibility of observing the onset of electron correlation effects as the insulator volume fraction is increased close to the percolation threshold. Third, by using mesoscopic sample sizes (of the order of 0.1–1 μm and at sufficient low temperatures so the inelastic scattering length is larger than the sample size), which are within the capability of modern lithographic techniques, one can observe not only the mean property of the conductance, such as the localization length, through sample-size variation, but also the conductance fluctuation and the form of the conductance distribution function. This information would be invaluable in the creation of a detailed picture of the Anderson localization phenomenon.

For a 2D electron gas, which is easily realizable nowadays using field-effect transistors, it is envisaged that by artificially inducing disorder in the transverse interfacial region, maybe by lithographic means, one can create locally insulating regions for the electron gas, thus causing scattering and localization. The advantage of this system, in addition to the two advantages mentioned above, is the variability of the Fermi energy (through the application of a gate voltage) and the associated electron density. The disadvantage, however, is that sample fabrication could be more difficult and time consuming.

In this work, we calculate the mesoscopic conductance of a disordered 2D metallic film using a quantum percolation model [6] in which a film with metal fraction p is simulated by conducting grains randomly occupying the sites of a simple square lattice with probability p. In practical terms, two-dimensionality implies a film thickness of ~100–400 Å for granular metals. Our results indicate four mesoscopic transport regimes. In the localized regime, i.e. sample size $L \gg$ localization length ξ_{loc}, the distribution of conductances is log–normal and the root-mean-square (RMS) conductance fluctuation is small compared with e^2/h, where e denotes the electronic charge and h is Planck's constant. In the opposite regime, i.e. $L <$ mean free path $l \ll \xi_{loc}$, the distribution is normal and the RMS fluctuation is larger than e^2/h. This is the ballistic transport regime (Ballistic transport does not mean no fluctuation since random geometry in each configuration can still induce random conductance). Between these two limits there are two regimes. For $l < L < 10l$, the transport is diffusive and the conductance distribution is still normal but the RMS fluctuation is greater than e^2/h. We denote this as the diffusive regime. For $10l \leqslant L < \xi_{loc}$, on the other hand, the distribution can be either normal or between normal and log–normal; the RMS fluctuation of the conductances is constant as a function of L and of the order of e^2/h. By definition, this is the regime of universal

conductance fluctuations (UCF). Our results, therefore, suggest experiments to verify these conductance regimes by looking at conductance and its variation with sample size, magnetic field, and p.

In the following, section 2 describes the model and the method of calculation. Results on mesoscopic conductance behaviour are presented in section 3, followed by concluding remarks in section 4.

2. Model description and the calculational approach

The most important characteristic of a mesoscopic sample is the absence of inelastic collisions. That means whatever the sample size the temperature must be low enough that the inelastic scattering length is larger than the sample size. However, that means that for mesoscopic samples there must be a new definition of the conductance, since in the traditional definition conductance is associated with dissipation, whereas now there is no dissipation in the samples. Landauer [7] was the first to show that in the absence of inelastic collisions the mesoscopic conductance can be obtained from the transmission and reflection coefficients of the sample in units of e^2/h. To relate this formulation of the conductance to the traditional definition, one then has to argue that the dissipation occurs in the resistive leads, i.e. dissipation is non-local. To calculate the conductance of a mesoscopic sample of a 2D granular metal film we consider a simple square lattice in which a fraction p of the sites is occupied by metal grains. We will only consider the regime $p > p_c = 0.593$ so that the metal grains always form a connected network. By including in our calculation the effects of a perpendicular magnetic field, the Hamiltonian of the quantum percolation model may be written in the following tight-binding form:

$$H = \sum_i \varepsilon_i |i\rangle\langle i| + t \sum_{[ij]} \exp\left(-\frac{2\pi i}{\varphi_0} \int_i^j \boldsymbol{A} \cdot \mathrm{d}\boldsymbol{l}\right) |j\rangle\langle i| \tag{1}$$

with

$$\varepsilon_i = \begin{cases} 0 \text{ if site } i \text{ is occupied by a metal particle} \\ \infty \text{ if site } i \text{ is occupied by an insulator} \end{cases}$$

where φ_0 denotes the unit of quantum flux, hc/e, $\boldsymbol{A}$ is the vector potential, t is the nearest-neighbour hopping matrix element, taken to be unity in this work, and i and j denotes the nearest-neighbour site indices of a square lattice with a lattice constant a, taken to be the typical granular particle size ~100 Å. In our numerical calculations the length is calibrated in units of a. In (1) the first term is the site energy term. Here we assign infinite site energy to insulators, which would prevent electrons from hopping to such sites. The second term describes the hopping between nearest-neighbour metal grains. Here the applied magnetic field can introduce a position-dependent phase to the hopping matrix element, obtained using the 'Peierls substitution' [8]. This model can be easily generalized to models of finite thicknesses, so that 3D effects may be considered.

In order to calculate the conductance, we connect two sides of a sample of size $L \times L$ by perfect leads, i.e. $p = 1$. The conductance is evaluated using the multichannel Landauer formula [9], i.e.

$$g = G/(e^2/h) = 4\left(\sum_{i=1}^{L_0} T_i\right)\left(\sum_{i=1}^{L_0} v_i^{-1}\right)\left(\sum_{i=1}^{L_0} (1 + R_i - T_i) v_i^{-1}\right)^{-1} \tag{2}$$

where L_0 denotes the number of propagating channels in the leads. The hard-wall

boundary condition is chosen along the transverse direction, y, with discrete transverse momentum index $k_y = \pi n/(L+2)$ where $n = 1, 2, \ldots, L+1$. The real solutions of k_x in the following dispersion relation determine the number of allowed channels L_0:

$$E/t = 2(\cos k_x a + \cos k_y a). \tag{3}$$

A factor of two, due to spins, has been included in (2). The values of T_i and R_i are related to the transmission and reflection matrices by

$$T_i = \sum_{j=1}^{L_0} |t_{ij}|^2 \tag{4a}$$

$$R_i = \sum_{j=1}^{L_0} |r_{ij}|^2 \tag{4b}$$

which in turn are calculated numerically using the recursive Green's function technique [10, 11] with

$$|t_{ij}|^2 = v_i v_i |G_{ij}^+(L+2, 0)|^2 \tag{5}$$

$$|r_{ij}|^2 = |i\sqrt{v_i v_i} G_{ij}^+(0, 0) - \delta_{ij}|^2 \tag{6}$$

where $G_{ij}^+(n, n')$ is the retarded Green's function with a source at n' of the x coordinate of channel j and a receiver at n of channel i. Positions 0 and $L+2$ are located inside the incoming and outgoing sides of the leads, respectively. The channel velocity v in (2), (5) and (6) is given by $\partial E/\partial k_x$ evaluated at $k_x(i)$. Technically, we have assigned a value of zero to any hopping matrix element connecting with empty site(s). Thus, the infinite site energy that appeared in (1) becomes irrelevant in the calculation.

3. Results and discussion

3.1. Statistical distributions of g

We would first like to discuss the statistical distribution of the dimensionless conductance g. Although there is a general belief that the distribution of g should be normal in the extended side but log–normal in the localized side [12, 13], yet, to our knowledge, there exists no systematic numerical study of this problem. In this work, we have systematically calculated the distribution of g as a function of p, sample size (L), and Fermi energy (E/t). Two characteristics of our calculated g are to be noted. The first is that in contrast to the classical 2D conductance, which is sample-size independent, the mesoscopic g is *L dependent due to the coherent backscattering effect.* Second, our calculated *g always goes to zero as $L \to \infty$*, in accordance with the known result that in a 2D random medium all waves are localized. Taking the ergodic hypothesis, which is believed to hold, we equate the fluctuations of g from sample to sample to that of a given sample as a function of E/t. Three types of distribution are found. When the sample size, L, is larger (but not much larger) than the elastic length, l, but much smaller than the localization length, ξ_{loc}, i.e. $l < L \ll \xi_{\text{loc}}$, the distribution of g is normal. In terms of g and Δg, the corresponding criterion for normal distribution is that $g \geqslant 3\Delta g$. In the opposite limit where the sample size is much greater than the localization length, i.e. $\xi_{\text{loc}} \ll L$, the corresponding distribution is log–normal. The intermediate regime is characterized by distributions which are neither normal nor log–normal.

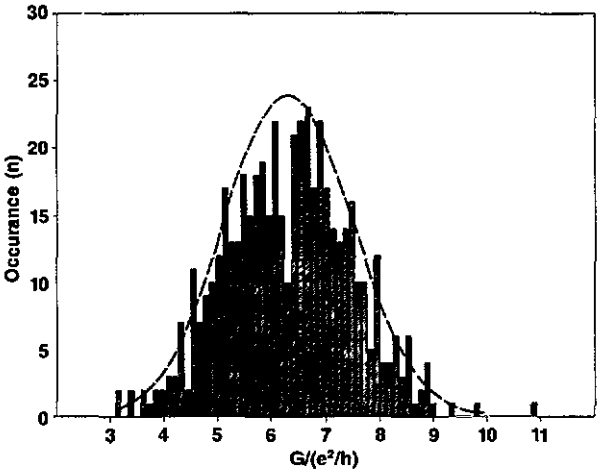

Figure 1. Histogram of the conductance distribution for 500 configurations. The parameter values are $E/t = 0.01$, $p = 0.95$, and $L = 60$. The broken curve is a Gaussian lineshape to guide the eye.

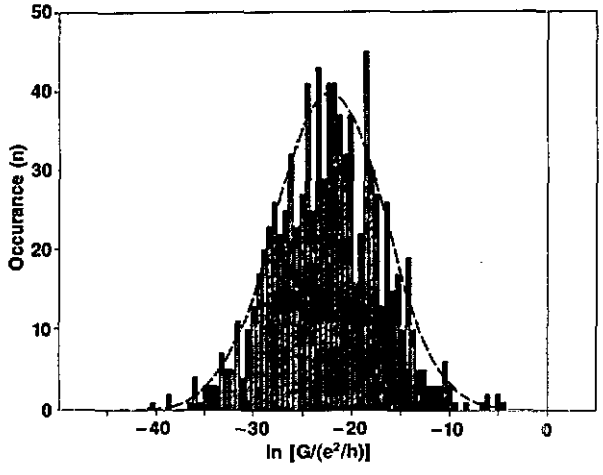

Figure 2. Histogram of the conductance distribution plotted as a function of $\ln[G/(e^2/h)]$ for 900 configurations. The parameter values are $E/t = 0.01$, $p = 0.75$, and $L = 60$. The broken curve is a Gaussian lineshape to guide the eye.

The three typical cases are shown in figures 1–3 for $L = 60$, $E/t = 0.01$ and $p = 0.95$, 0.85 and 0.75. At $p = 0.95$, the value of l is about 12, and the localization length is expected to be much greater than 60. The distribution of g for 500 configurations is shown in figure 1 and is seen to be a very good Gaussian. At $p = 0.75$, the localization length is only 2.7 (much smaller than sample size $L = 60$, or 0.6 μm, if the grain size is ~100 Å) and the histogram of $\ln(g)$ is shown in figure 2 for 900 configurations. The distribution is found to be a good Gaussian in terms of $\ln(g)$, i.e. the distribution of g is log-normal in this regime. However, the case of $p = 0.85$ belong to the intermediate

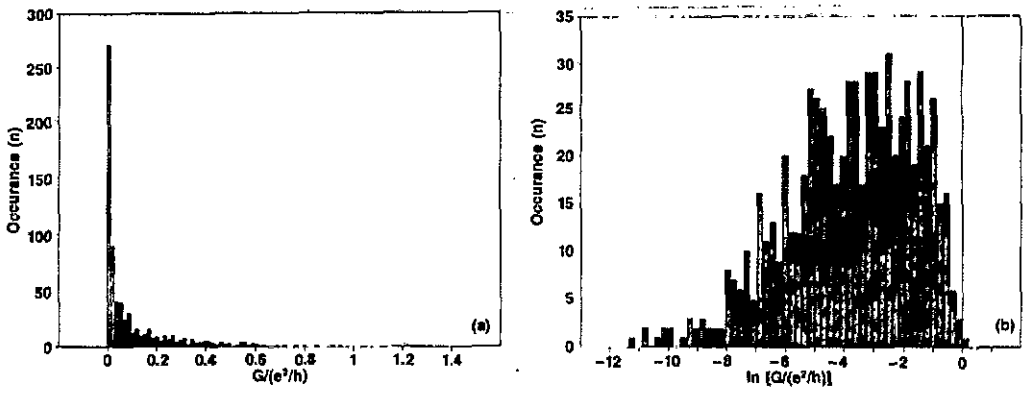

Figure 3. (*a*) Histogram of conductance distribution for 700 configurations. The parameter values are $E/t = 0.01$, $p = 0.85$, and $L = 60$. (*b*) Histogram of the conductance distribution plotted as a function of $\ln[G/(e^2/h)]$ for 700 configurations. The parameter values are the same as for (*a*).

regime with $\xi_{loc} = 16$, which is not much smaller than the sample size (60×60). The distribution, with 700 configurations, is shown in figure 3 in terms of both g and $\ln(g)$; they are clearly non-Gaussian. The peculiar distribution can be viewed as being intermediate between normal and log–normal, i.e. the large conductance part is normal (figure 3(*a*)) while the smaller conductance part is log–normal (figure 3(*b*)).

3.2. First moment of the distribution: localization length

For a fixed p, one can get the mean value of $\ln g$, $\langle \ln g \rangle$, for various sample sizes, L. Its behaviour as a function of L is plotted in figure 4 for three values of $p = 0.75$, 0.80 and 0.85. Near-linear variation is observed. From the relation $\xi_{loc} = -\mathrm{d}L/\mathrm{d}\langle \ln g \rangle$, we obtain the values of ξ_{loc} as 2.7, 5.0 and 16.4 for $p = 0.75$, 0.80, and 0.85, respectively. In these cases, ξ_{loc} is small compared with our sample sizes, $L = 30$–90. When p becomes greater than 0.85, ξ_{loc} is found to increase drastically.

3.3. Second-moment of the distribution: conductance fluctuations

The RMS conductance fluctuation, $\Delta g = \sqrt{\langle g^2 \rangle - \langle g \rangle^2}$, has been calculated for different Fermi energies and as a function of L and $p = 0.65$–0.90. The behaviour of Δg can be roughly divided into two energy regions: (i) a less localized (higher conductance) region with $0.3 < E/t < 2.0$ and (ii) a more localized (lower conductance) region with E/t outside the region of (i).

For $E/t = 0.5$, the RMS value of Δg is plotted in figure 5 as a function of sample size, L, for different values of p ranging from 0.65 to 0.90. 100 to 6000 configurations have been generated for each L and p combination. Those configurations which do not percolate across the sample are dropped. In general, less configurations are required for good statistics as L becomes large and p approaches one. Although Δg is in general a smoothly decaying function of L, there exists a region where the value of Δg decays very slowly even for large L, e.g. $0.75 < p < 0.85$ and $L > 30$. The value of Δg in this region agrees well with the theoretical UCF value of 0.862 in 2D. For p close to one, a much larger L is required to reach the region of UCF since the elastic scattering length increases.

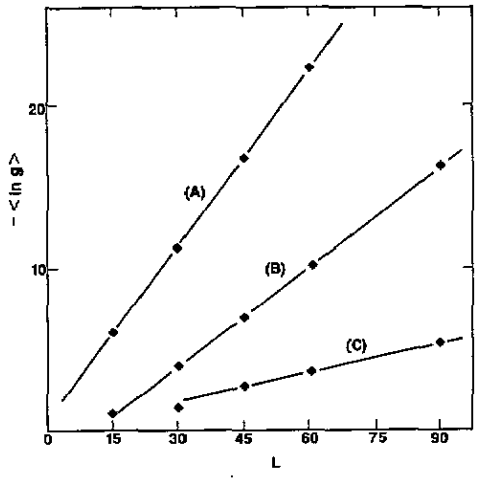

Figure 4. The averaged value of $-\ln(g)$ plotted as a function sample size L. The data points show a linear behaviour. The inverse of the slope gives the localization length. For (A) $p = 0.75$, (B) $p = 0.80$, and (C) $p = 0.85$. The value of E/t is 0.01.

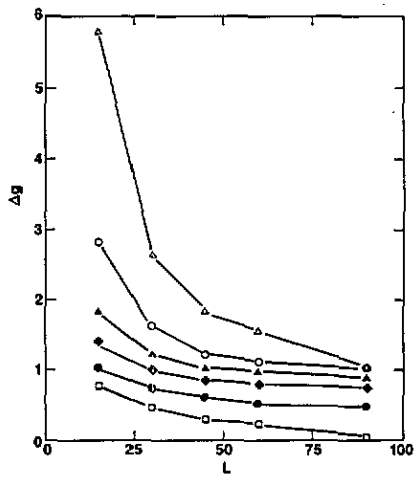

Figure 5. The RMS dimensionless conductance fluctuation Δg plotted as a function of sample size L for various values of p: '△', for $p = 0.90$, '○' for 0.85, '▲' for 0.80, '◆' for 0.75, '●' for 0.70, and '□' for 0.65. The value of E/t is 0.5.

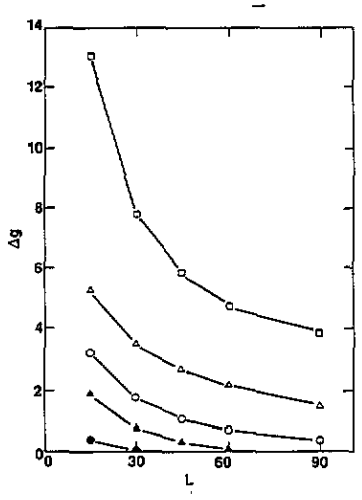

Figure 6. The RMS dimensionless conductance fluctuation Δg plotted as a function of sample size L for various values of p: '□' 0.95; '△', 0.90; '○', 0.85; '▲', 0.80; '●', 0.75. The value of E/t is 0.01.

On the other hand, as p becomes close to the percolation threshold p_c (= 0.593) the localization length becomes smaller and the region of UCF is also limited to small L. Both of these features can be seen in curves for $p = 0.9$ and 0.7 in figure 5.

The situation is quite different in the more localized region, $0 < E/t < 0.3$. At $E/t = 0.01$, the curves of Δg for different values of p are shown in figure 6. There is no region of constant Δg that can be identified. This may be understood as follows. For $p \leqslant 0.85$ the localization length estimated from figure 5 is smaller than L. That means that for the size of samples considered, the system is already localized, with the consequent result of decreasing Δg as L increases. On the other hand, when p is

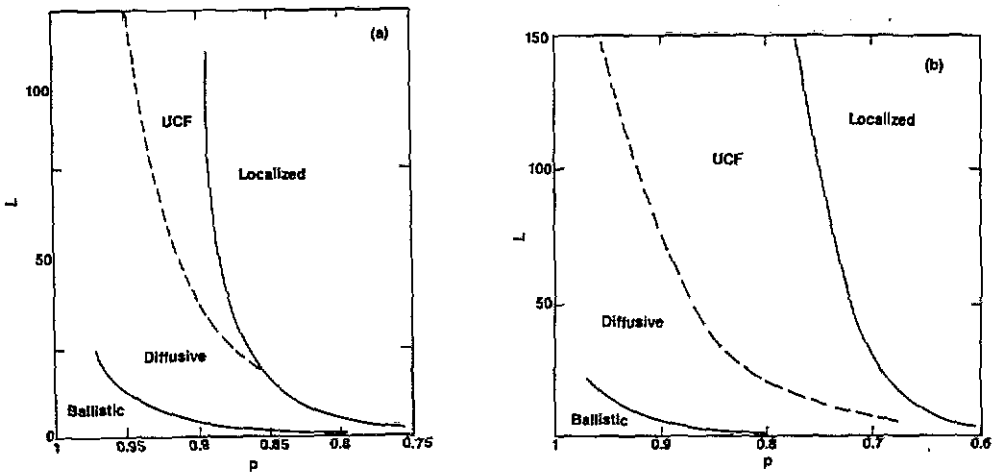

Figure 7. Transport regimes of the 2D quantum percolation model as a function of L and p. The upper full curve denotes the localization length, the lower full curve denotes the mean free path. The broken curve denotes ten times the mean free path. (*a*) $E/t = 0.01$, (*b*) $E/t = 0.5$.

greater than 0.85, the localization length quickly increases beyond the sample size. The corresponding increase in the elastic scattering length, which is proportional to $(1-p)^{-1}$ in the weak disorder limit, pushes the region to UCF to much larger sample sizes ($L > 90$). A rough estimate of elastic scattering length can be made by using the number of effective channels [13]. In the extended region ($L <$ localization length), we have $g = N_{\text{eff}} = 2L_0 l/L$ where L_0 is the number of allowed channels. From this relation, the values of l are found to be about $l = 12$, 4 and 1.6 for $p = 0.95$, 0.9, and 0.85, respectively. Thus, it requires at least $L > 120 (= 10l)$ in order to see UCF for $p = 0.95$. This is consistent with the corresponding curves shown in figure 6.

If the same considerations are now applied to the cases shown in figure 5, we found that the values of l at $E/t = 0.5$ are about 7, 3.7, 2 and 1.3 for $p = 0.90$, 0.85, 0.80 and 0.75, respectively. Although these numbers are about a factor of two higher than the corresponding numbers in the case of $E/t = 0.01$, the localization length, ξ_{loc}, is also much greater. From finite size scaling the localization length is found to be ≈ 30 for $p = 0.70$. A rough estimate gives $\xi_{\text{loc}} \approx 100$ and 250 for $p = 0.75$ and 0.80. Thus our results confirm the theoretical prediction that the UCF exists in regions where $10l < L < \xi_{\text{loc}}$. We have also shown that outside of the UCF region one obtains $\Delta g > 1$, decreasing with L for $L < 10l$. For $L > \xi_{\text{loc}}$, $\Delta g \ll 1$ and decreases with increasing L.

3.4. Conduction regimes

Summarizing all the results stated above, in figure 7 we show the conduction regimes as a function of sample size L and metal fraction p. Four regimes are delineated, from ballistic ($L < l$), to diffusive ($l < L < 10l$), to UCF ($10l < L < \xi_{\text{loc}}$), to localized ($L > \xi_{\text{loc}}$). In figure 7(*a*) we show the case for which the Fermi energy is in the more localizing energy range of $E/t = 0.01$, and in figure 7(*b*) show the case for which $E/t = 0.5$ is in the energy range in which the electron tends to be more delocalized.

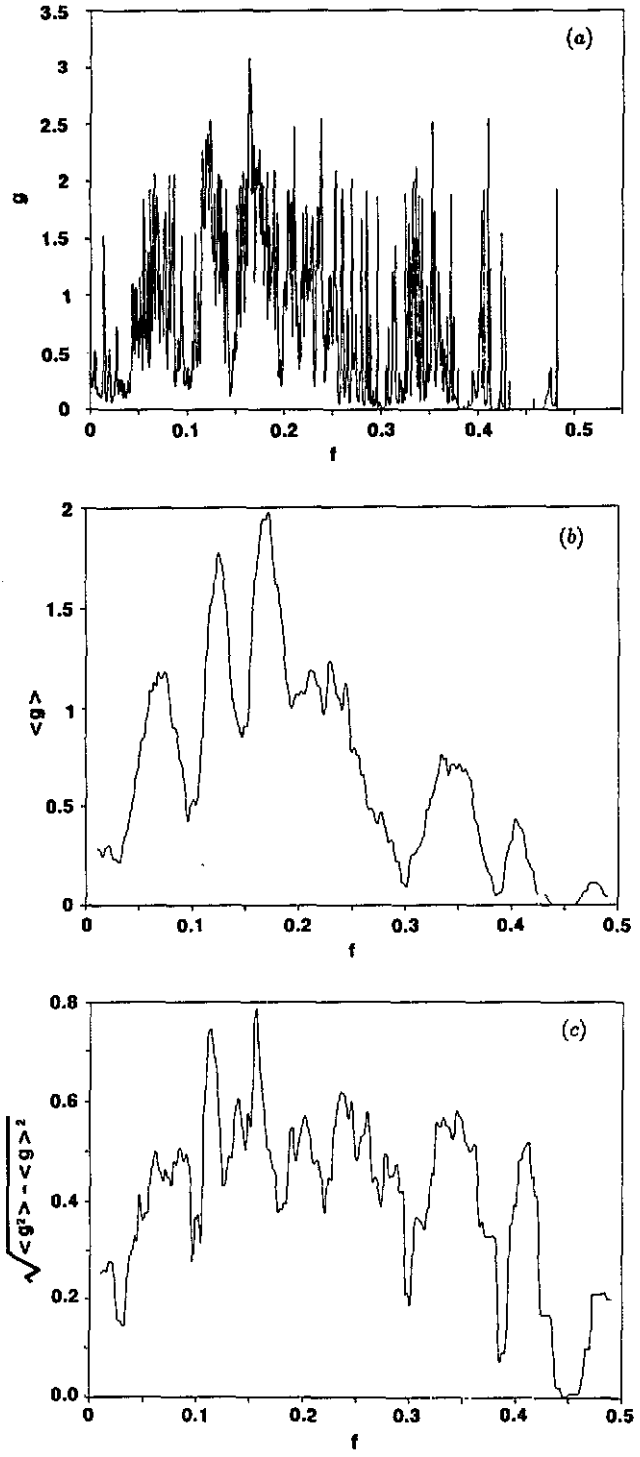

Figure 8. (*a*) Calculated g as a function of the fraction, f, of quantum flux φ_0 for $p = 0.7$, $L = 60$ and $E/t = 0.5$. (*b*) The mean $\langle g \rangle$ calculated with a moving window size of $\Delta f = 0.02$. (*c*) The RMS conductance fluctuation Δg calculated with a moving window size of $\Delta f = 0.02$.

3.5. Magnetic field dependence

Whereas in the results described above we have used different samples for obtaining the conductance distribution, it is also possible to look at the conductance fluctuations in a single sample by varying the magnitude of the applied perpendicular magnetic field H. The idea in such a case is that the magnetic field can introduce random phases (due to the random geometry) which can directly affect the interference pattern of the electronic wavefunctions. By varying H, one can essentially regard the same system at two very different H values as being two different samples. At the same time, magnetic field also introduces a magnetic length $L_H = \sqrt{hc/4eH}$, where c is speed of light. When L_H becomes less than the physical sample size, then heuristically, L_H replaces L in determining the conductance. That implies that by increasing H one can scan across the different conduction regimes shown in figure 7 for a fixed p. Figure 8 shows the calculated results for $p = 0.7$, $L = 60$ and $E/t = 0.5$ for g, $\langle g \rangle$ and Δg as functions of $f = Ha^2/\varphi_0$, where $\varphi_0 = hc/e^2$ denotes the quantum flux. For particle size $a \simeq 100$ Å, $f = 0.14$ corresponds to $H \simeq 7$ T. It is seen that there are indeed large fluctuations in g as a function of f. The Δg, calculated by using moving windows of width $\Delta f = 0.02$, show an initial rise, a relatively flat region signalling the UCF region and a final decline, probably when L_H becomes less than l. However, the variation of $\langle g \rangle$ with f may *not* be translated into localization length since the magnetic field destroys the time-reversal invariance, and thereby weakens the coherent backscattering effect that is essential for localization.

4. Concluding remarks

It has been more than thirty years since the concept of Anderson localization was first proposed [14]. Up until now, while weak localization effects, i.e. those associated with coherent backscattering, have been widely observed [15], strong localization of electrons has only been seen in the context of metal–insulator transitions in doped semiconductors and some other materials systems [16], where the presence of electron–electron correlation effect inevitably obscures the signature of the Anderson localization phenomenon. In this work we have studied in some detail the mesoscopic electronic transport properties of thin metallic films using the 2D quantum percolation model. Based on these results we propose experiments to directly verify the Anderson localization. Two key requirements of the proposed experiments are: (i) small sample size, which may be achieved by lithographical techniques; and (ii) low measuring temperatures so that the inelastic scattering length is larger than the sample size (based on estimates, an inelastic scattering length of 1 μm for granular metals would mean $T \simeq 0.1$ K). Since the Anderson localization is a generic aspect of wave behaviour in random media, its actual observation is expected to have important implications for both basic science and practical applications. This is especially the case in view of the continually decreasing size of microelectronic systems and hence the increasing significance of the electron quantum/wave nature. By presenting this proposal, it is our hope that added attention may be focused on verifying this basic phenomenon of wave-randomness interactions.

Acknowledgment

The authors wish to thank K Unruh for helpful discussions. This work is supported by ONR contract #N00014-88-K-0003.

References

[1] Lee P A, Stone A D and Fukuyama H 1987 *Phys. Rev.* B **35** 1039
[2] See Cody G D, Geballe T H and Sheng P (ed) 1990 *Physical Phenomena in Granular Materials (MRS Symp. Proc. 195)* (MRS, Pittsburgh, Pennsylvania) and references therein
[3] Sheng P, Abeles B and Arie Y 1973 *Phys. Rev. Lett.* **31** 44
Abeles B, Sheng P, Arie Y and Coutts M 1975 *Adv. Phys.* **24** 407
[4] Sheng P and Klafter J 1983 *Phys. Rev.* B **27** 2583
[5] Beamish J R, Patterson B M and Unruh K M 1990 *Physical Phenomena in Granular Materials (MRS Symp. Proc. 195)* ed G D Cody, T H Geballe and P Sheng (Pittsburgh, PA: Materials Research Society) p 129
[6] Zhang Z Q and Sheng P 1991 unpublished
[7] Landauer R 1957 *IBM J. Res. Dev.* **1** 223
[8] Peierls R E 1933 *Z. Phys.* **80** 763
[9] Buttiker M, Imry Y, Landauer R and Pinhas S 1985 *Phys. Rev.* B **31** 6207
[10] Lee P A and Fisher D S 1981 *Phys. Rev. Lett.* **47** 882
[11] Stone A D 1985 *Phys. Rev. Lett.* **54** 2692
[12] Lee P A and Ramakrishnan T V 1985 *Rev. Mod. Phys.* **51** 287
[13] Imry Y 1986 *Europhys. Lett.* **1** 249
[14] Anderson P W 1958 *Phys. Rev.* **109** 1492
[15] See, for example,
Sheng P (ed) 1990 *Scattering and Localization of Classical Waves in Random Media,* (Singapore: World Scientific) and references therein
[16] Mott N F and Davis E A 1971 *Electronic Processes in Non-Crystalline Materials* (Oxford: Clarendon)